GMR
The Original

FORMULATION OF DOSATINIB ENCAPSULATED NANOCARRIERS BY BOX-BEHNKEN DESIGN OF EXPERIMENTS AND DETERMINATION OF EFFICACY IN MCF-& CELL LINE

Gaurav Karodadeo[1], Shikha Jaiswal[2*]

[1] Research Scholar, Department of Pharmacy, Oriental University, Indore (M.P).
[2] Supervisor, Department of Pharmacy, Oriental University Indore (M.P).
*Corresponding Author: Gaurav Ramesh Karodadeo, gauravkarod@gmail.com

ABSTRACT
Dosatinib is a strong chemotherapy medicine that is used to treat many types of cancer, such as ovarian, breast, and non-small cell lung cancer. However, it is hard to employ in clinical settings since it doesn't dissolve well in water, has serious side effects, and may cause multi-drug resistance. Researchers are exploring for innovative ways to distribute drugs to get around these problems, and Dosatinib-loaded hyaluronic acid (HA) micelles are getting a lot of interest. HA is a naturally occurring polymer that is very soluble in water, safe for living things, and breaks down easily. It is found in the extracellular matrix. HA can self-assemble into micelles in water when it is chemically changed with hydrophobic substances. After that, hydrophobic medicines like Dosatinib can be put in the midst of these HA micelles. Dosatinib -loaded hyaluronic acid Pluronic (DSB-HA-PF127) micelles represent a significant advancement in cancer nanomedicine, offering advantages over conventional chemotherapy through targeted distribution, enhanced efficacy, and reduced unwanted effects. This study seeks to enhance the efficacy of Dosatinib by encapsulating it within hyaluronic acid micelles, thereby prolonging its half-life in the bloodstream. The Box-Behnken experimental design was utilised to enhance the formula.

KEYWORDS: Dosatinib, Dosatinib-loaded hyaluronic acid Pluronic micelles, Box-Behnken experiment design

INTRODUCTION

Dosatinib is an orally available short-acting dual ABL/SRC tyrosine kinase inhibitor (TKI). It potently inhibits BCR-ABL and SRC family kinases (SRC, LCK, YES, FYN), but also c-KIT, PDGFR-α and PDGFR-β, and ephrin receptor kinase. Initially intended for chronic myeloid leukemia treatment, it has shown potential against various cancers such as lung, prostate, and ovarian cancer (1,2)

Dosatinib is a multifaceted compound belonging to several chemical categories, including secondary and tertiary amino compounds, organochlorine compounds, aminopyrimidines, 1,3-thiazoles, monocarboxylic acid amides, N-arylpiperazines, and N-(2-hydroxyethyl) piperazines, as per IUPAC nomenclature. Its chemical name is N-(2-chloro-6-methylphenyl)-2 -[[6-[4-(2-hydroxyethyl)-1-piperazinyl] -2-methyl-4-pyrimidinyl] amino]-5-thiazole carboxamide, monohydrate, with a molecular formula of $C_{22}H_{26}ClN_7O_2S.H_2O$ and a formula weight of 506.02 for the monohydrate, while the anhydrous free base weighs 488.01(3,4)

Bristol-Myers Squibb developed dosatinib (BMS-354825, Sprycel), gaining FDA approval in 2006 for inhibiting multiple tyrosine kinases. It's used as a second-line treatment for specific types of leukemia with resistance to imatinib (5)

dosatinib presents as a crystalline white powder with pH-dependent aqueous solubility ranging from 18.4 mg/ml at pH 2.6 to 0.008 mg/ml at pH 6.0. Its solubility is limited in various solvents. Additionally, it binds strongly to serum proteins (>90 %), undergoes oxidative metabolism primarily via CYP3A4, and has an oral bioavailability of 14 %–34 %. However, its clinical use is hindered by adverse effects like gastrointestinal disorders, hemorrhage, increased endothelial permeability causing peripheral edema and pleural effusion [6,7].

Efforts to enhance dosatinib's therapeutic efficacy and mitigate its adverse effects focus on efficient delivery systems like nanoparticles. Nanoparticle-based drug delivery systems offer advantages such as increased drug solubility, improved pharmacokinetics, targeted tumor delivery via the enhanced permeability and retention (EPR) effect, and the ability for functional modifications. Utilizing nanocarriers could significantly improve dosatinib's aqueous solubility, tumor-targeting capabilities, and reduce its adverse effects, potentially maximizing its therapeutic utility [[8], [9], [10]].

Various nanocarriers have been extensively researched to enhance the delivery of dosatinib, a drug used in leukemia treatment, resulting in better inhibition of tumor cell growth compared to using dosatinib alone. For

instance, albumin nanoparticles were explored as carriers to mitigate dosatinib-induced endothelial hyperpermeability, thereby improving its effectiveness against leukemia [11]. Additionally, layered polymer-coated carbon nanotubes were studied to control dosatinib delivery and enhance its efficacy against U-87 glioblastoma cells [12]. In a different approach, dosatinib was incorporated into gold nanoparticles, either functionalized with specific molecules or short genetic material complementary to a particular gene overexpressed in leukemia cells, resulting in enhanced drug effectiveness with reduced toxicity [13]. Another study utilized magnetic protein micelles to improve dosatinib delivery to triple-negative breast cancer cells [14]. Recently, polymeric nanoparticles made from poly (cyclohexene phthalate) were reported as effective carriers for dosatinib delivery [15]. However, while these nanocarriers can enhance drug uptake and retention within cancer cells due to their small size, they lack specificity and precise control over drug release.[16]

2. MATERIAL AND METHODS

Sun Pharmaceutical Pvt. in Baroda gave us a sample of DOSATINIB as a gift. We got hyaluronic acid from BFC Lab. Loba Chemi Pvt. Ltd. gave us ethanol, dimethyl sulfoxide (DMSO), and dimethylformamide (DMF). The rest of the substances were of analytical grade.

2.1 Preparation of DSB-HA-PF127 micelles

The DSB-HA-PF127 micelles were made using a modified version of the previously described thin film hydration approach (TFH) [9]. Briefly, 4 milligrammes of dosatinib (DSB) diluted with 3 millilitres of acetonitrile., and 50 mg of HA dissolved in 10 mL of water separately. Then both the solution subject to ultrasonication for 10 cycles of three minutes (30 minutes). About 10 mg of Pluronic F127 was added to HA solution with heating to get homogeneous solution. Both the solution then transferred to rotary evaporator for further evaporation of sol vent at 50°C for 30 minutes. This results into the thin film formation which was subject to hydration using miliQ water. After that, the DSB-HA-PF127 micelles were made by stirrin them constantly on a magnetic stirrer at 40°C for an hour. After that, it was passed through a membrane filter with 0.22 μm pores. Prepared micelles were then subject to further analysis.

2.2 Quality by Design (QbD) based design of experiment

The QbD-based experiment design is the most effective way to create experiments for the systematic formulation technique. Therefore, a trial with a QbD-based design was employed to accomplish the study's suggested aim, and the related reaction characteristics were used to gauge the influence of the formulation and process components.

2.3 Experimental Design

In the current study, the Box-Behnken type of experimental strategy technique was used to systemically enhance the effectiveness of the formula and processing parameters [10]. Independent variables including drug concentrations (X1, mg), hyaluronic acid concentrations (X2, mg), and temperature (X3, ℃) have all been considered in order to improve the formula. Their influence on trapping effectiveness was also quantified. As shown in Table 4, seventeen distinct batches were made with every conceivable combination of medication and hyaluronic acid at the ideal temperature in order to get an ideal formulation with the maximum entrapment efficiency.

Equation (1), which uses a statistical framework with polynomial and interaction factors, was used to evaluate the response.

$$Y = b_0 + b_1X_1 + b_2X_2 + b_3X_3 + b_{11}X_1^2 + b_{22}X_2^2 + b_{33}X_3^2 + b_{12}X_1X_2 + b_{23}X_2X_3 + b_{13}X_1X_3 \quad \text{Eq. (1)}$$

In this case, b0 reflects the average result from all 17 trials, b1 is the expected coefficient for the factor X1, and Y is the dependent variable. The primary impacts (X1, X2, and X3) reflected the mean results of altering each element individually from a minimal to maximal number. The terms of interaction (X1X2, X2X3, and X1X3) showed that the answer varied when all three variables were altered all at once. Terms involving polynomials (X12, X22, and X32) were introduced in order to explore non-linearity.

The three factors' values at the level and the overall make-up of both Box-Behnken design batches were as seen in tables 2 and 3.

Table 2: The study's factors, together with their coded levels and "Real" values

	Levels		
Variables	-1	0	+1
Independent	**Real values**		
Conc. of Drug (X_1, mg)	20	40	60
Conc. of Hyaluronic Acid (X_2, mg)	50	100	150
Temperature (°C)	40	50	60

Dependent
Entrapment efficiency (Y, % w/w)

Table 3: Box-Behnken design of experiment formulation batches

Sr. No.	Batches	X1	X2	X3
1.	F1	60	100	40
2.	F2	60	100	60
3.	F3	40	50	60
4.	F4	40	100	50
5.	F5	60	50	50
6.	F6	20	50	50
7.	F7	20	100	40
8.	F8	60	150	50
9.	F9	20	150	50
10.	F10	40	100	50
11.	F11	40	50	40
12.	F12	40	100	50
13.	F13	40	150	40
14.	F14	40	100	50
15.	F15	40	150	60
16.	F16	20	100	60
17.	F17	40	100	50

2.4 Characterization of HA-DSB micelles

2.4.1 Particle Size and zeta potential analysis

The particle sizes of the DSB-HA-PF127 micelles were examined using photon correlation spectroscopy (PCS) and dynamic light scattering on a Zetasizer® nano (Model: Zen 3600, Malvern Instruments, Malvern, UK) equipped with a 5-mW helium neon laser with an output wavelength of 633 nm [11, 12]. The evaluations were taken at a 90° angle, at 25 °C, and for a minimum of 40 to 80 seconds. Water served as the dispersant. Micelles derived from phospholipids have an electrophoretic mobility-based zeta potential that was calculated using Smoluchowski's equation [13]. Three duplicates of each measurement were made.

2.4.2 DSC analysis

DSC was used to analyse the polymorphism state of dosatinib, hyaluronic acid, pluronic and their physical combination. Dried nitrogen gas was supplied at a flow rate of 80 mL/min as a purging agent. Inside the instrument chamber was an aluminum pan with around 5 mg of powdered material. a single heating cycle that increased the temperature by 10 °C per minute from 40 °C to 400 °C [13]. Their highest points, found examined using TA software.

2.4.3 FTIR

The interaction between the ingredients needed to make DSB-HA-PF127 was investigated, and the physical mixing infrared spectra of dosatinib and hyaluronic acid were acquired. An FTIR spectrophotometer (FTIR-8300) was used to record the FTIR spectra of dosatinib, HA, pluronic and their physical mixture. Pretreatment was briefly administered to the dosatinib, HA, pluronic to prepare them for Fourier transform infrared (FTIR) analysis, as well as their physical mixes. At a ratio of 1:100, these substances were mix together evenly in the presence potassium bromide (KBr) of FTIR quality. Then leter, they had 45 scans with a 4 cm–1 resolution and analyses between 4,500 and 400 cm–1 [14].

2.4.4 Entrapment efficiency

The DSB-HA-PF127 micelles' entrapment efficiency was assessed by means of a range of techniques that were documented across published works[15, 16]. One milliliter of DSB-HA-PF127 was added to the Centricon® reservoir (Model: YM-100, Amicon, Millipore, Bedford, MA, USA). The filtrate containing free dosatinib was collected after the DSB-HA-PF127 micelles were through a centrifuge 40 minutes at 15,000 rpm. To ascertain the quantity of dosatinib, The purified diffusion was further mixed with methanol and put through a UV analysis. The UV-spectrophotometric analysis was employed to ascertain the dosatinib concentration in the filtrate following centrifugation (Cf) and the total concentration of dosatinib (Ct).

The entrapment efficiency was calculated using the following equation (2);

$$\text{Entrapment efficiency (\%)} = \frac{C_t - C_f}{} \times 100$$

$$\frac{}{C_t}$$ Eq. (2)

2.4.5 Drug content

DSB-HA-PF127 micelles loaded with dosatinib were detected using the UV technique, which was first described by Rarokar et al. in 2022 [13]. For 20 minutes, DSB-HA-PF127 micelles containing 10 mg of dosatinib in 100.0 mL of ethanol were dissolved through shaking strongly. Five minutes were spent sonicating the solution. 1.0 mL of the filtrate was taken out after the the solution through a filter using a 0.45 µ filter. It was then reduce the concentration with 10 mL of distilled water and put through a spectrophotometric analysis at 230 nm.

2.4.6 Scanning electron microscopy

Following the formation of the spheres, little bit of the DSB-HA-PF127 micelle formulation that had been tuned stood on a microscope slide and let lack of moisture [17]. The sphere's surface area on microscope slide was covered together with a modest coating of palladium using an auto fine coater (Model: JFC1600, Jeol Ltd., Tokya, Japan). A scanning electron microscope (Model: JSM-6390LV, Jeol Ltd., Tokyo, Japan) with a digital camera and a 10 KV accelerating voltage was used to investigate the palladium-coated samples.

2.5 *In-vitro* DOSATINIB release study

The dosatinib discharge from the DSB-HA-PF127 micelles was assessed by calculating the
drug's diffusion utilising a Franz diffusion cell through a cellophane membrane. The cell comprised two compartments.: two separate compartments, one for donors and one for receptors. A semipermeable barrier, earlier on Already enabled, divided these two compartments. The donor compartment above the membrane was filled with the DSB-HA-PF127 micelle formulation. A release medium of about 18 milliliters of phosphate buffer saline solution (PBS) pH 7.4 was maintained at 37±0.5°C inside the receptor compartment. At at regular intervals, partial solutions of the releasing agent were removed and swapped out with an equivalent amount of new-release material. The amounts of drugs released media at several
periods were examined using UV light [17].

2.6 Statistical analysis

The data was expressed using the mean±standard deviation (SD). A two-way analysis of variance (ANOVA) and a Bonferroni post-test were employed for the statistical evaluation, which was conducted using GraphPad® Prism® software version 5.03 (San Diego, CA). The P value was considered less than 0.05 if there were significant differences between the means.

RESULTS AND DISCUSSION

Drug-Excipient Compatibility Studies

DSC is a popular and well-recognized analytical method for examining how different materials interact chemically. It is also helpful for obtaining data on stability, compatibility, melting, and deterioration. Peak alterations, peak start time, peak shape, and relative area all reveal information about the interaction between the medication and the excipient and the creation of new entities. As illustrated in Figure 1A, Pure DSB's DSC thermogram revealed a prominent the peak of endothermic activity observed at around 288.6 °C, which corresponds to the fusion temperature of DSB. At around 84.5 °C, hyaluronic acid (HA) displayed distinct endothermic peaks (see Figure 1B). At at 55.9 °C, the Pluronic® F127 displayed distinct endothermic peaks (see Figure 1C). A little and insignificant alteration within the thermal behaviour of DSB when there is HA and Pluronic® F127 was found by the physical mixtures' DSC analysis, DSB, HA, and Pluronic F127 (1:1) (see Figure 1D). with In the physical preparations of the corresponding polymers with DSB, Pluronic® F127's melting signals (endotherm) were easily discernible. Therefore, any physical contact or evident conflicting nature of the medication as well as polymers was ruled out due to the lack of all other types of heat transfer events across the whole ambient temperature. So, the findings from the DSC showed these polymers were appropriate for use in the composition that were produced.

The compatibility between polymers and drugs is demonstrated by the three thermograms of the drug, polymer, and the combination of both.

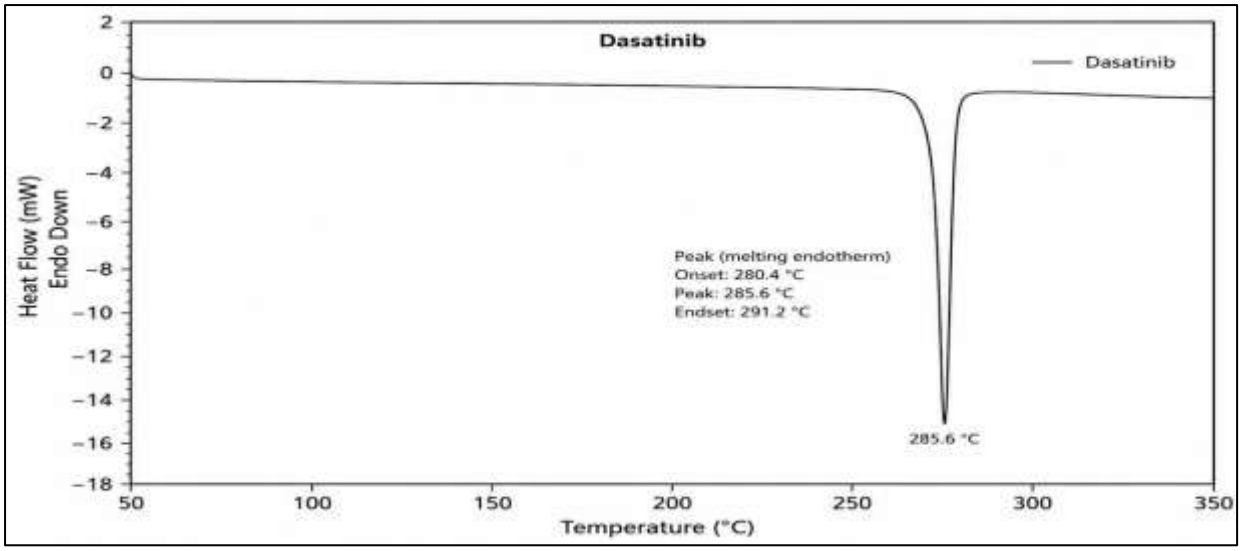
Dasatinib
Dasatinib
Heat Flow (mW)
Endo Down
Peak (melting endotherm)
Onset: 280.4 °C
Peak: 285.6 °C
Endset: 291.2 °C
285.6 °C
Temperature (°C)

(A)

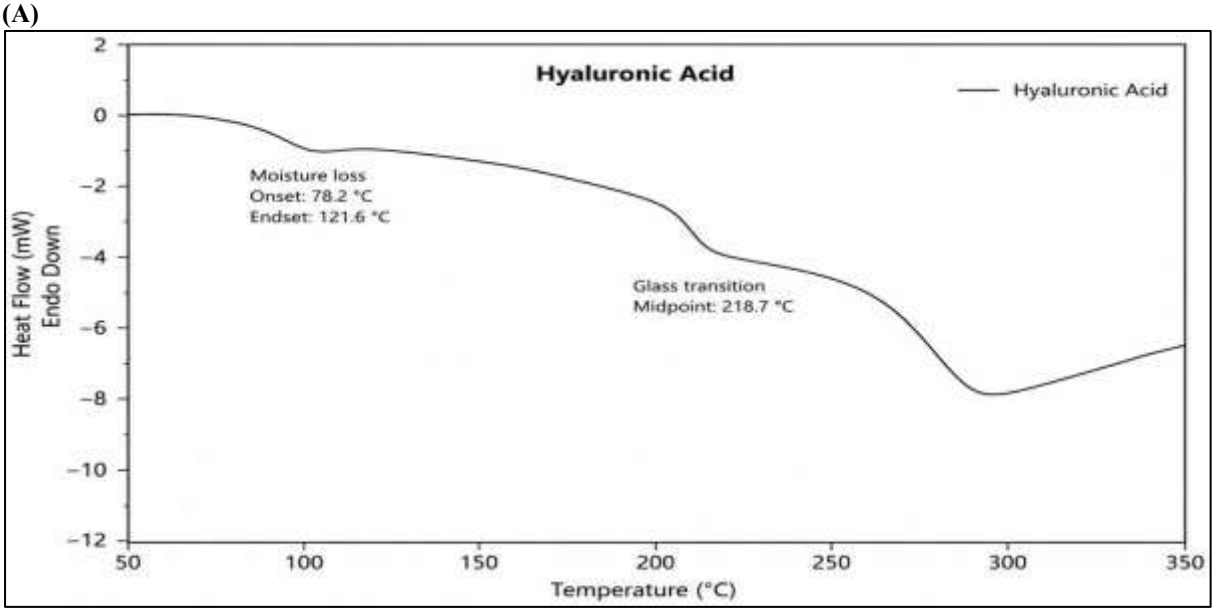
Hyaluronic Acid
Hyaluronic Acid
Heat Flow (mW)
Endo Down
Moisture loss
Onset: 78.2 °C
Endset: 121.6 °C
Glass transition
Midpoint: 218.7 °C
Temperature (°C)

(B)

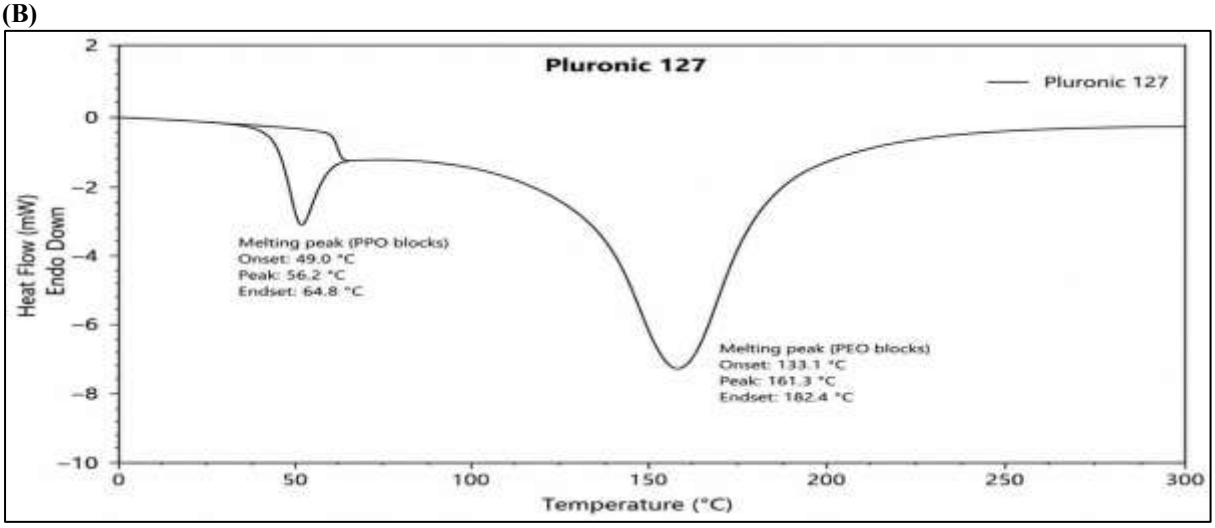
Pluronic 127
Pluronic 127
Heat Flow (mW)
Endo Down
Melting peak (PPO blocks)
Onset: 49.0 °C
Peak: 56.2 °C
Endset: 64.8 °C
Melting peak (PEO blocks)
Onset: 133.1 °C
Peak: 161.3 °C
Endset: 182.4 °C
Temperature (°C)

(C)

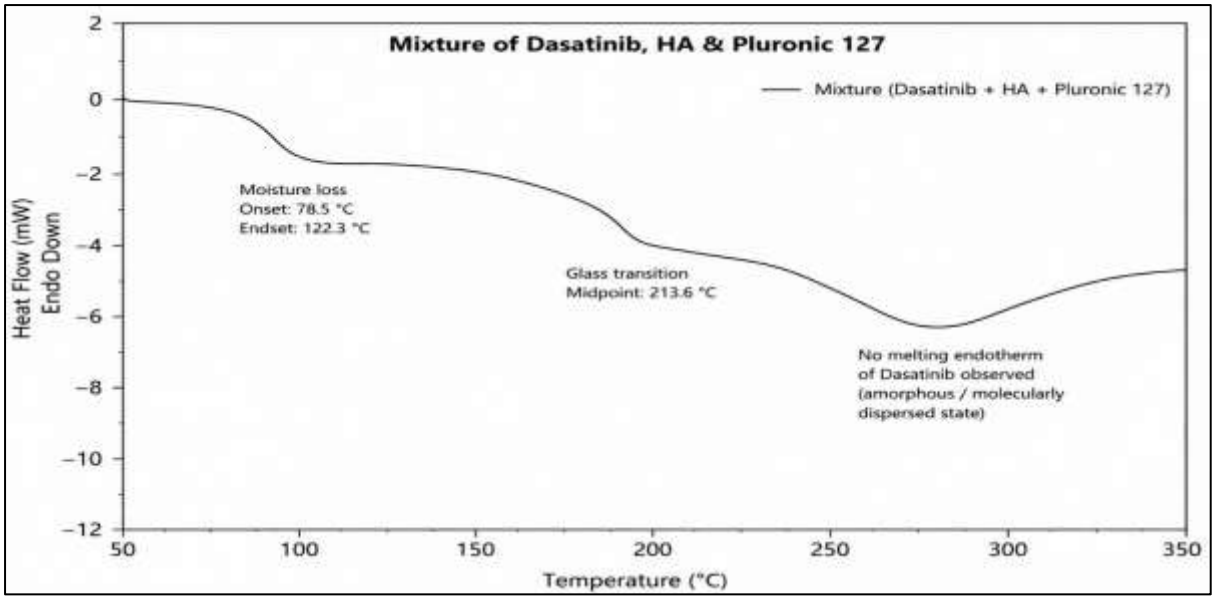

(D)

Figure 1: DSC thermogram of DSB (A) HA (B) Pluronic F127 (C) and physical mixture of DSB, HA and Pluronic F127 (D)

FTIR

Figure 2 depicted the FTIR spectra of DSB (2A), HA (see Figure 2B), Pluronic® F127 (see Figure 2C) or the binary combination of it (see Figure 2D). The distinctive peaks in the pure DSB spectrum are roughly located at wave numbers 2360, 2340, 1690, 1570, 1500, 1180, 1050, 800–700 cm^{-1}, which correlate to the hydroxyl group (-OH), ester (C=O), and amino group (-NH). The peaks were discovered to be comparable to the results that had been previously published [18, 19]. The distinctive peaks in HA's FTIR spectra are located at 2360, 2340, 1649, 1572, 1522, 1400, 1375, 1032, 670, 651 and 420. The distinctive peaks of the Pluronic® F127 were typically located at 2882, 2360, 2340, 1469, 1402, 1342, 1279, 1244, 1146, 1059, 981, and 841cm-1. The physical mixture of DSB, HA, and Pluronic® F127 was subjected to FTIR analysis, which showed that C=O stretching peaks, amino groups (-NH), and hydroxyl groups (-OH) were all conserved in the spectrum (see Figure 2D). The distinct spectra as well as those derived from their physical composition did not, therefore, exhibit any discernible differences. Accordingly, the FTIR study's results showed no conclusive proof of a reaction between DSB and the polymer in question.

Accordingly, the FTIR study's results showed no conclusive proof of a reaction between the used polymers and dosatinib trihydrate.

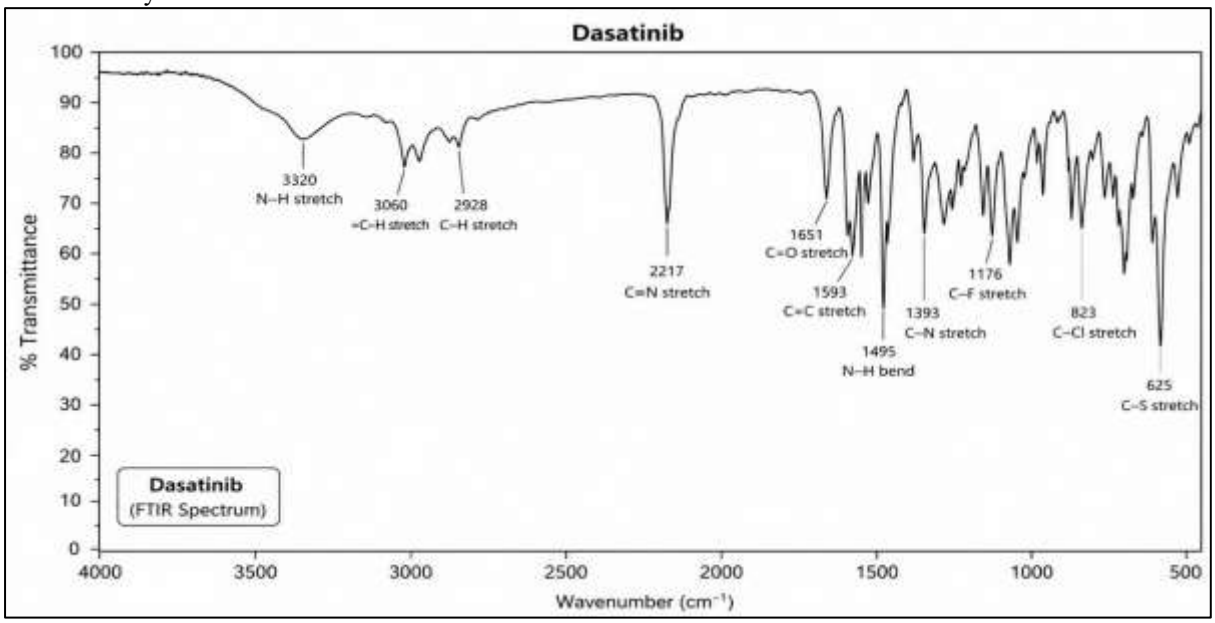

(A)

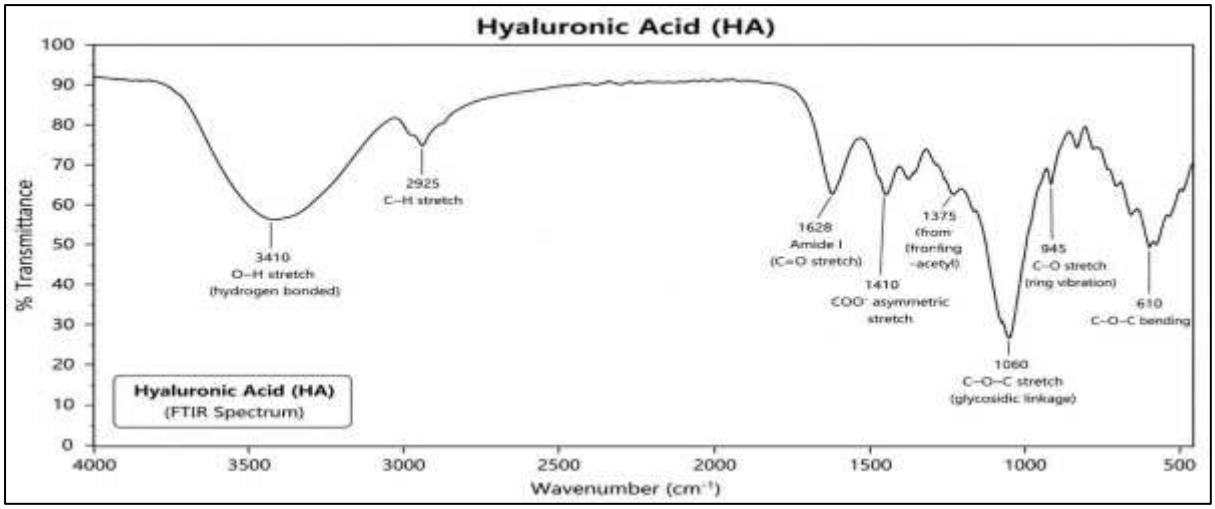

(B)

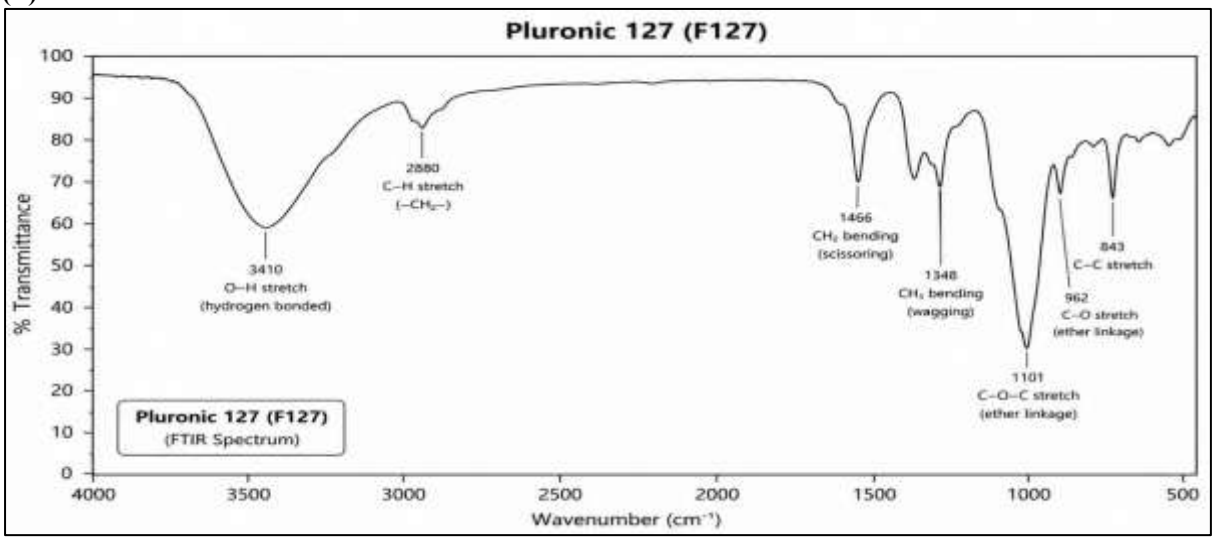

(C)

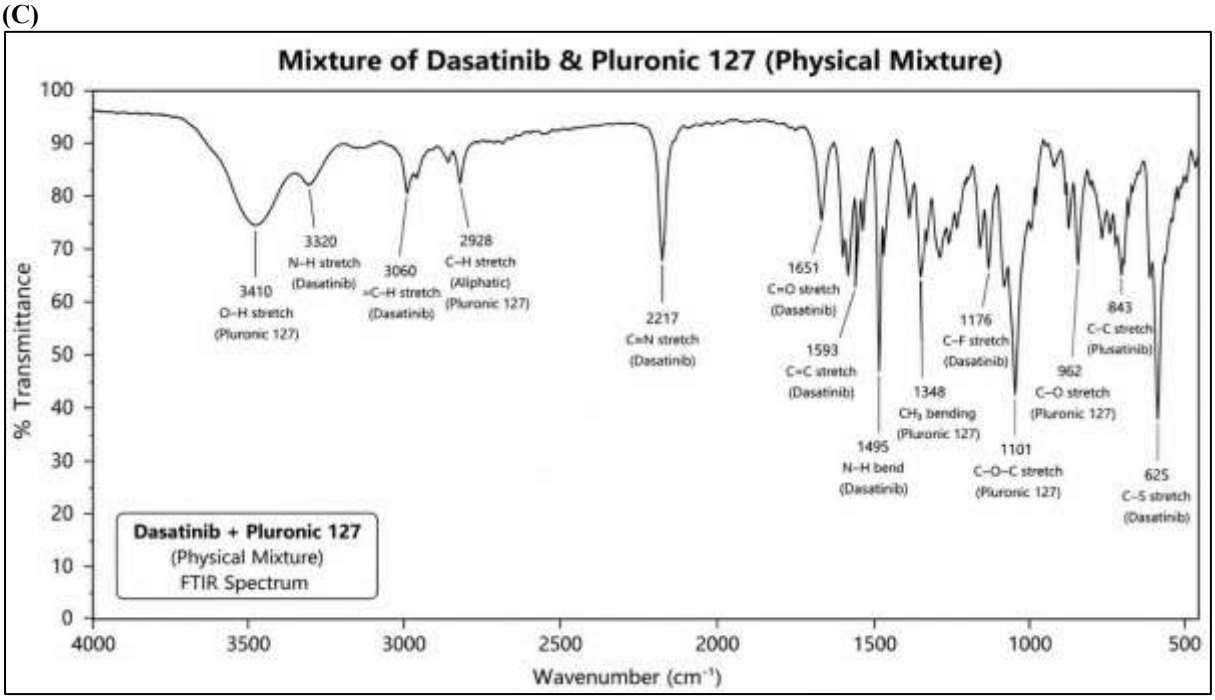

(D)

Figure 2: FTIR spectra for DSB (A) HA (B) Pluronic F127 (C) and physical mixture of DSB and Pluronic F127 (D)

Optimization of formula

Three-dimensional surface plots of entrapment efficiency (Y, %) against drug and HA concentration (X1), drug concentration and temperature (X2), and HA concentration and temperature (X3) are shown in Figure 3 (D, E, and F). Figure 3 (A, B, and C) shows a contour plot of entrapment efficiency (Y, %) against drug and hyaluronic acid concentration, drug concentration and temperature, and hyaluronic acid concentration and temperature. Figure 3 (A, B, C, D, E, and F) and Equation 3 demonstrated that while X2 had a positive effect on Y, independent variables X1 and X3 had a negative effect on %EE.

FIT SUMMERY

Linear	0.0295	0.0004	0.3689	0.1793	
2FI	0.7439	0.0002	0.2710	-0.2904	
Quadratic	**< 0.0001**	**0.0796**	**0.9705**	**0.8336**	**Suggested**
Cubic	0.0796		0.9890		**Aliased**

ANOVA for Quadratic model
Response 1: EE

Model	4134.25	9	459.36	59.55	< 0.0001	significant
A-Conc. of Drug	393.40	1	393.40	51.00	0.0002	
B-Conc. of HA	1615.96	1	1615.96	209.48	< 0.0001	
C-Temperature	31.20	1	31.20	4.05	0.0842	
AB	51.84	1	51.84	6.72	0.0358	
AC	63.20	1	63.20	8.19	0.0243	
BC	124.32	1	124.32	16.12	0.0051	
A^2	106.57	1	106.57	13.82	0.0075	
B^2	1264.69	1	1264.69	163.94	< 0.0001	
C^2	337.73	1	337.73	43.78	0.0003	
Residual	54.00	7	7.71			
Lack of Fit	42.43	3	14.14	4.89	0.0796	not significant
Pure Error	11.57	4	2.89			
Cor Total	4188.25	16				

The Model F-value of 59.55 implies the model is significant. There is only a 0.01% chance that an F-value this large could occur due to noise.
P-values less than 0.0500 indicate model terms are significant. In this case A, B, AB, AC, BC, A^2, B^2, C^2 are significant model terms. Values greater than 0.1000 indicate the model terms are not significant. If there are many insignificant model terms (not counting those required to support hierarchy), model reduction may improve your model.
The Lack of Fit F-value of 4.89 implies there is a 7.96% chance that a Lack of Fit F-value this large could occur due to noise. Lack of fit is bad -- we want the model to fit. This relatively low probability (<10%) is troubling.

Std. Dev.	2.78		**R^2**	0.9871
Mean	75.97		**Adjusted R^2**	0.9705
C.V. %	3.66		**Predicted R^2**	0.8336
			Adeq Precision	23.7125

The Predicted R^2 of 0.8336 is in reasonable agreement with the Adjusted R^2 of 0.9705; i.e. the difference is less than 0.2.
Adeq Precision measures the signal to noise ratio. A ratio greater than 4 is desirable. Your ratio of 23.713 indicates an adequate signal. This model can be used to navigate the design space.

CODED FORMULA
EE= 90.712 + -7.0125 * A + 14.2125 * B + 1.975 * C + -3.6 * AB + -3.975 * AC + -5.575 * BC + -5.031 * A^2 + -17.331 * B^2 + -8.956 * C^2

The equation in terms of coded factors can be used to make predictions about the response for given levels of each factor. By default, the high levels of the factors are coded as +1 and the low levels are coded as -1. The coded equation is useful for identifying the relative impact of the factors by comparing the factor coefficients.

ACTUAL FORMULA
EE= -356.811 + 2.00932 * A + 2.37223 * B + 11.0635 * C + -0.0036 * AB + -0.019875 * AC + -0.01115 * BC + -0.0125775 * A^2 + -0.0069324 * B^2 + -0.08956 * C^2
The equation in terms of actual factors can be used to make predictions about the response for given levels of each factor. Here, the levels should be specified in the original units for each factor. This equation should not be used to determine the relative impact of each factor because the coefficients are scaled to accommodate the units of each factor and the intercept is not at the center of the design space.

For specific values forecasts for each component on the response can be derived from the coded factors by applying equation 3. By default, the numbers +1 and -1 represent the elevated and decreased levels of the factors, in that order.The relative relevance of the elements might be determined using the equation with codes by comparing the component values.

Table 4: Seventeen batches of DSB-HA-PF127 micelles by employing Box-Behnken Design

Batch	**Factor 1 A: Concentration of drug (%w/v)**	**Factor 2 B: Concentration of HA (%w/v)**	**Factor 3 C: Temperature (°C)**	**Response 1 Entrapment Efficiency (%)**
1	60	100	40	71.4
2	60	100	60	67.5
3	40	50	60	60
4	40	100	50	89.5
5	60	50	50	48.7
6	20	50	50	55
7	20	100	40	78
8	60	150	50	74.5
9	20	150	50	95.2
10	40	100	50	89
11	40	50	40	45
12	40	100	50	93
13	40	150	40	80
14	40	100	50	91.96
15	40	150	60	72.7
16	20	100	60	90
17	40	100	50	90.1

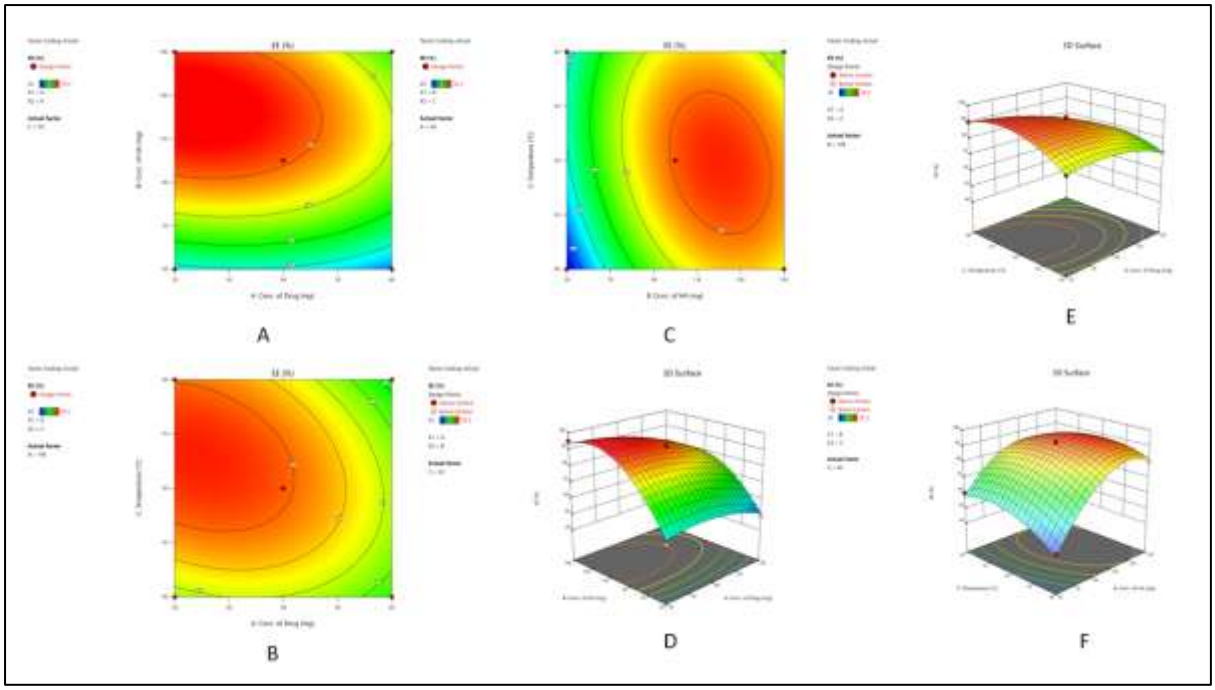

Figure 3: Contor plot of entrapment efficiency (%) against A) concentration of DSB and HA B) concentration of DSB and temperature and C) concentration of HA and temperature; 3D surface plots of entrapment efficiency (%) against D) concentration of DSB and HA, E) concentration of DSB and temperature and F) concentration of HA and temperature.

Validation of Model

For assessing the optimisation capacity of models produced in accordance with the findings of the central composite design, DSB-HA-PF127 micelles were made with an ideal concentration of drug (DSB), concentration of HA and temperature were 0.1 %w/v, 3 %w/v and 50 ℃ respectively. The % Bias when it comes to the estimated and real entrapment efficiency values for for DSB-HA-PF127 micelles were determined to be below ±3.0%, confirming that significancy of the model.

$$Bias\ (\%) = \frac{predicted\ value - observed\ value}{predicted\ value} \times 100 \qquad \text{Eq (4)}$$

Physicochemical characterization of HA-PF127-DSB micelles

Particle size, polydispersity index (PDI) and the zeta potential

Since they had increased surface area/volume ratio, smaller particles facilitate the release of the encapsulated medication from the DSB-HA-PF127 micelles through surface erosion and diffusion. Additionally, this has the benefit of allowing the DSB-HA-PF127 micelles to enter and pass past the physiological drug barriers. Prior research has proposed that the lymphatics would absorb the larger particles (less than 5 mm), whereas endocytosis would allow the smaller particles (less than 500 nm) to pass past the membrane of epithelial cells [20]. The hydrodynamic diameter of the nanocarriers affects the effectiveness of passive targeting as well [21].

Figure 5 (A and B) displays the zeta potential, polydispersity index (PDI), and particle size of DSB-HA-PF127 micelles. As shown in Figure 5A, about the typical size of DSB-HA-PF127 micelles was determined to be 149.9±2.58. Therefore, the average particle dimension of the DSB-HA-PF127 micelles was observed to be only slightly increased by the DSB loading. DSB-HA-PF127 micelles were discovered to have a polydispersity index of 0.152±0.017. Referring to Figure 5B, the zeta potential of DSB-HA-PF127 micelles was determined to be -18 mV.

Furthermore, DSB-HA-PF127 micelles' low polydispersity index value suggested a limited particle size distribution [22]. Another crucial indicator of the DSB-HA-PF127 micelles' stability is their zeta potential. In a buffer solution, A high zeta potential indicates that the surface of the material is heavily charged electrically DSB-HA-PF127 micelles, which can prevent the micelles from aggregating and create strong repelling forces between particles [23, 24, 25]. While smaller particle sizes are more likely to have a lengthy circulation half-life and a higher likelihood of tumor localization, a lowest possible zeta potential of more than -30 mV is generally regarded as appropriate and suggestive of strong physical stability [26].

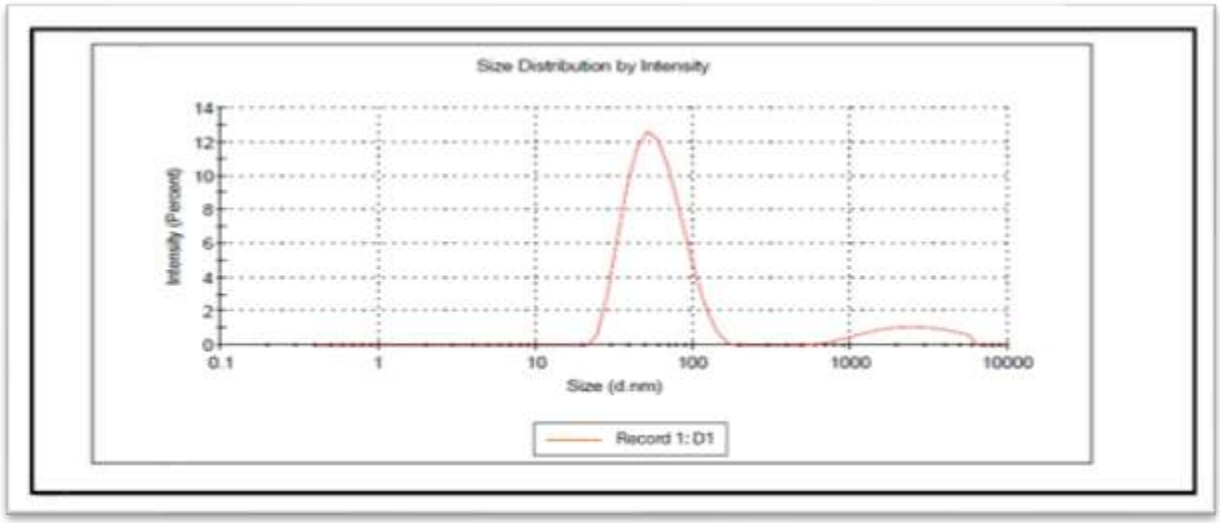

(A)

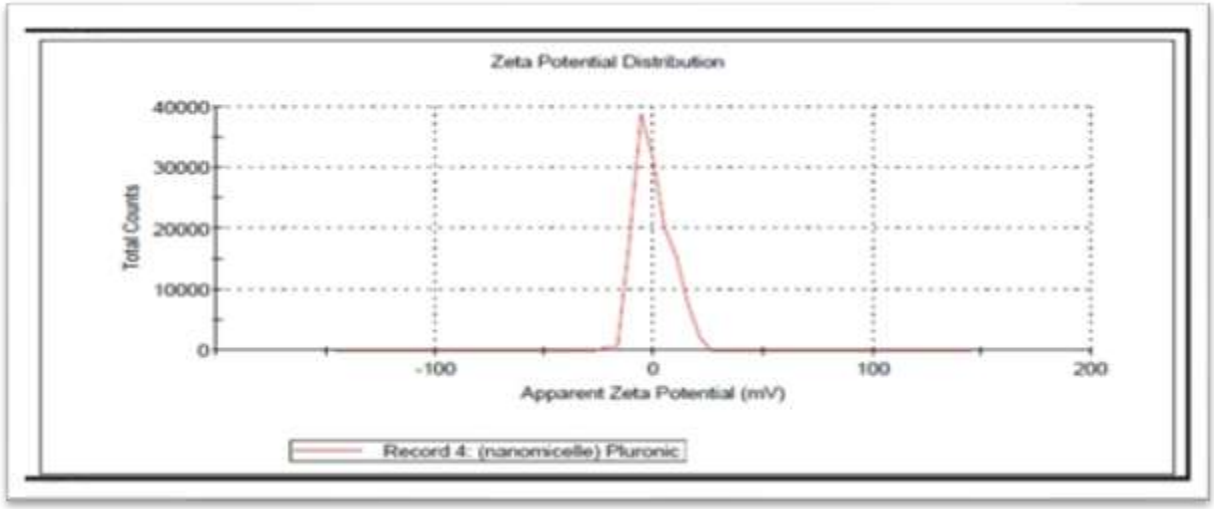

(B)

Figure 5: Particle size (A) and zeta potential (B) of DSB-HA-PF127 micelles

XRD

The crystalline nature of the chemical conjugated with the other polymer structure is determined using X-ray diffraction (XRD). The XRD spectra of HA, PF127, and DSB-HA-PF127 micelles are shown in Figs. 6A, 6B, and 6C. The characteristic peaks at the Bragg angle, 2_ h = 12.40, 15.724, 18.122, 20.01, 22.67, and 24.991 with intensity 654, are seen in the pluronic® diffractogram.Peaks at Bragg angle 2 h = 19.42, 21.99, 31.02 (with a higher intensity of 5879), and 34.210 (intensity = 3108) were visible in the XRD diffractogram of HA-PF127. The XRD study's findings showed that DSB-HA-PF127 micelles were formed, which was consistent with earlier research [27]. The XRD pattern of DSB-HA-PF127 micelles (see Fig. 4C) showed that the distinctive HA peaks had vanished, leaving only a few peaks remaining. The XRD of the DSB-HA-PF127 micelles, on the other hand, showed the distinctive peaks of PF127.

C

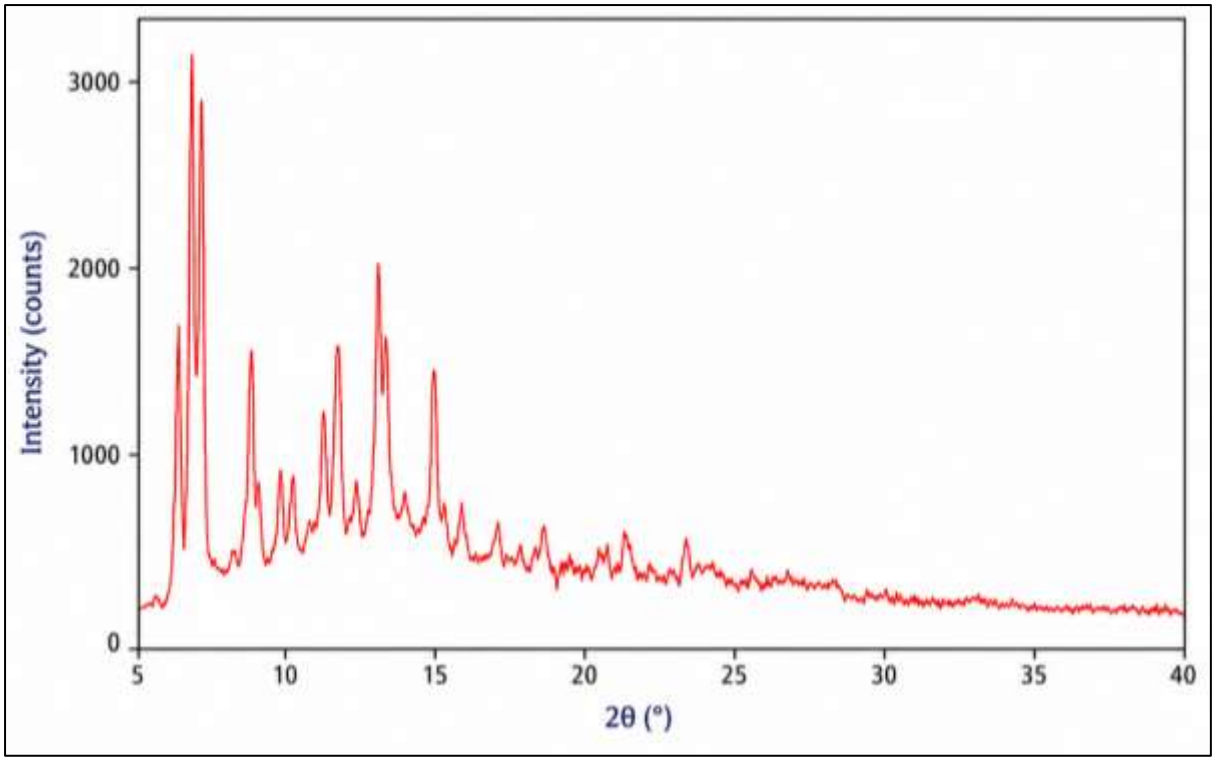
Intensity (counts)
3000
2000
1000
0
5
10
15
20
25
30
35
40
2θ (°)

(A)

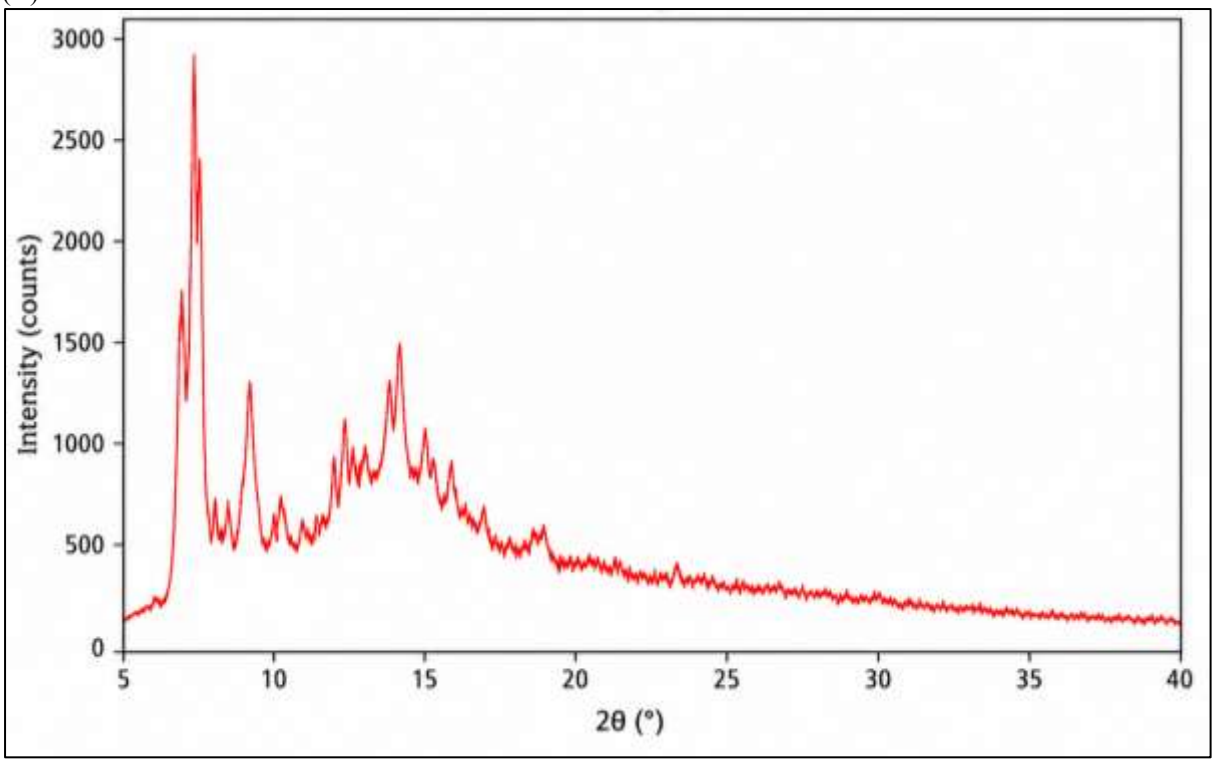
Intensity (counts)
3000
2500
2000
1500
1000
500
0
5
10
15
20
25
30
35
40
2θ (°)

(B)

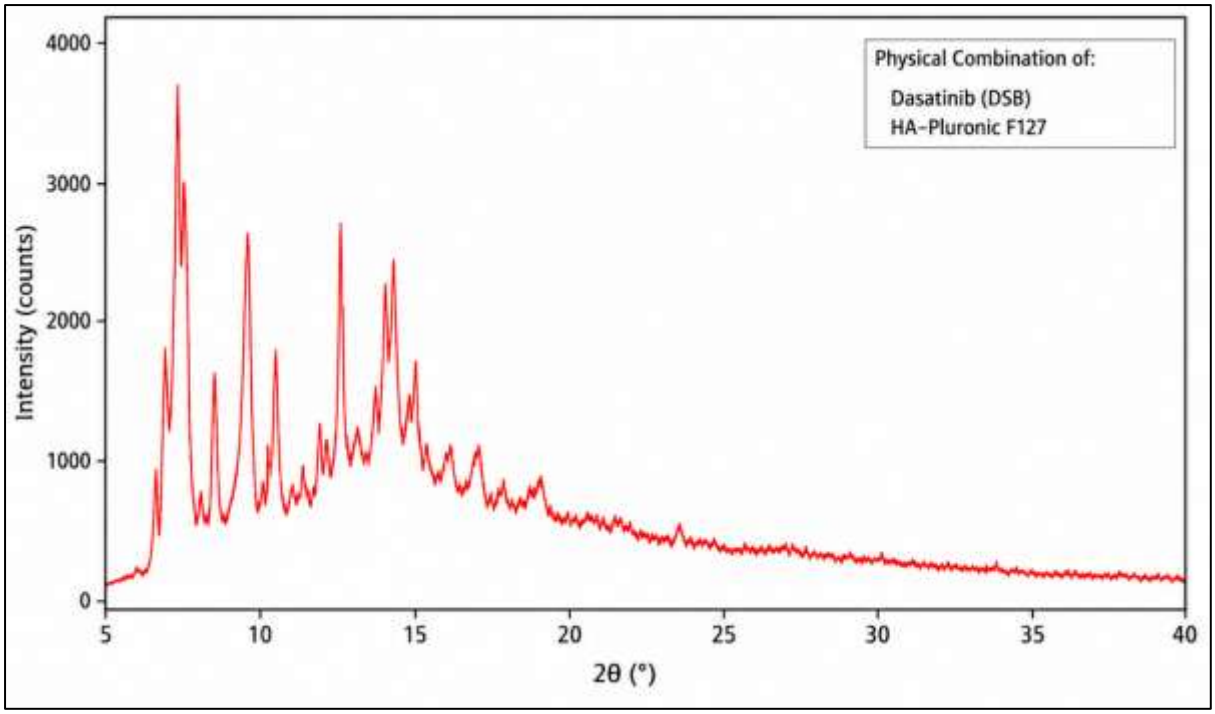

(C)

Figure 6: XRD of DSB (A), HA (B) and physical combination of DSB and HA-Pluronic F127 (C)

Entrapment efficiency

Important measures for drug delivery systems include drug entrapment efficiency. Especially with pricey medications, this is true. DSB-HA-PF127 micelles were discovered to have an entrapment efficiency of 95.89±2.5 (% w/w), meaning that the majority of DSB was encapsulated in these micelles.

Drug content

The drug content for optimized DSB-HA-PF127 micelles was found to be 97.28 ± 1.2.

***In-vitro* DSB Release from** DSB-HA-PF127 micelles

Figure 7 illustrates the DSB release pattern from the DSB-HA-PF127 micelles as assessed by the Franz diffusion cell. Within one hour, the DSB-HA-PF127 micelles showed their first burst release (30.56%). After then, DSB was gradually released from the DSB-HA-PF127 micelles over a 12-hour period. Over 95.66% of DSB was released from the DSB-HA-PF127 micelles after 12 hours, whereas over 93.85% of DSB was liberated in just 6 hours from the DSB hydroalcoholic solution. According to the findings, DSB-HA-PF127 micelles the possibility of being put to use in controlled medication delivery systems.

Table 5: Drug release of DSB from DSB solution and DSB-HA-PF127 micelles

Time (h)	DSB-solution	DSB-HA-PF127 Micelles
0	0	0
2	55.65	30.56
4	81.46	48.392
6	93.85	64.558
8	-	78.34
10	-	86.168
12	-	95.66

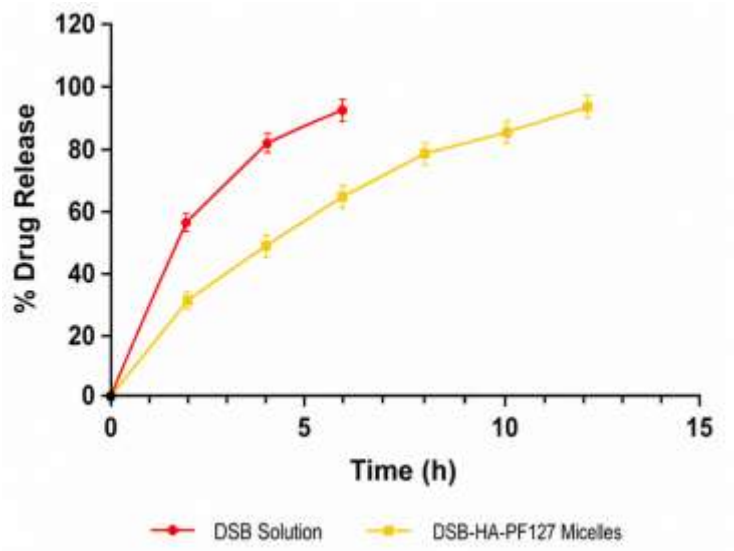

Figure 7: % drug release of SB from DSB solution and DSB-HA-PF127 micelles

Scanning Electron Microscopy (SEM)

The DSB-HA-PF127 micelles were analyzed by SEM for surface morphology. The electron micrographs at different magnifications at 100x, 700x and 5000x revealed the formation of some spherical shape DSB-HA-PF127 micelles formation as shown in figure 8A and 8B.

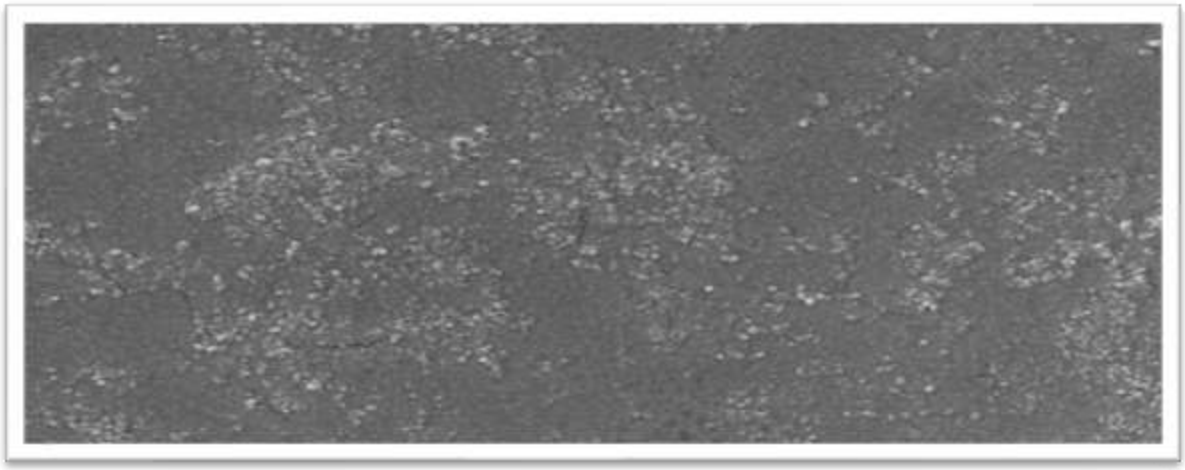

(A)

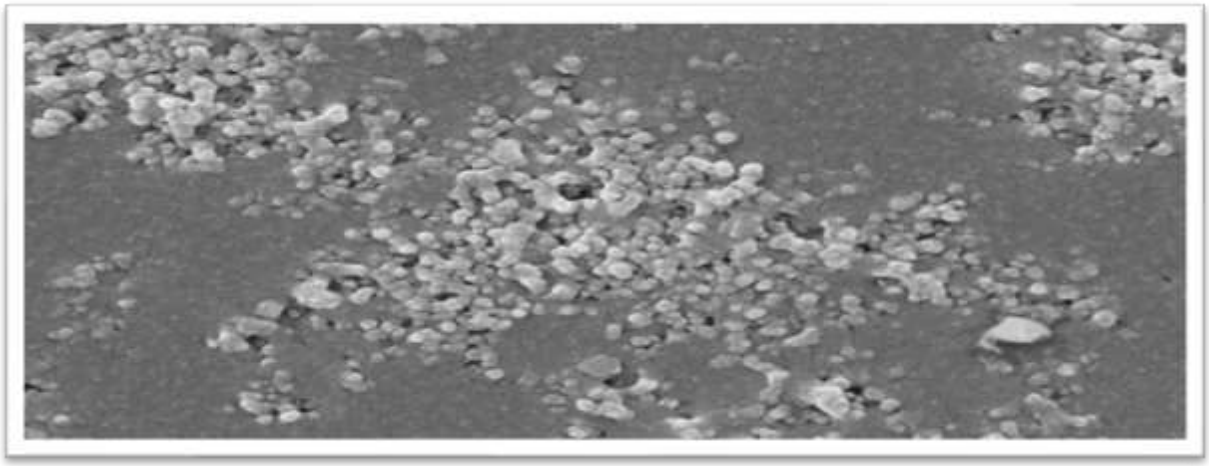

(B)

Figure 8: SEM image of DSB-HA-PF127 micelles at various magnification shows somewhat spherical shape micelles

Cytotoxicity studies (MTT Assay)

We utilized the MTT test to perform a cytotoxicity of cells investigation using human breast adenocarcinoma cell lines (MCF-7) applicable to both the DSB hydroalcoholic solution and the (DSB HA Sol.) and DSB-HA-PF127 micelles at different doses. Relative proliferation after treated with acetonitrile as well as blank-HA-PF127 micelles and relative inhibition after treatment with DTSBHA-PF127 micelles and DSB HA solution were determined (**Figure 9A**). According to the findings of the cell cytotoxicity investigation, for every concentration of 0.01, 0.1, 1, 10, 100, and 1000 µM, the percentage of human breast cancer cells the DSB HA solution, indicating higher cytotoxicity of the formulation towards cells. The IC50 values for DSB-HA-PF127 micelles and DSB HA solution were determined to be 0.51µM and 0.89µM, respectively.

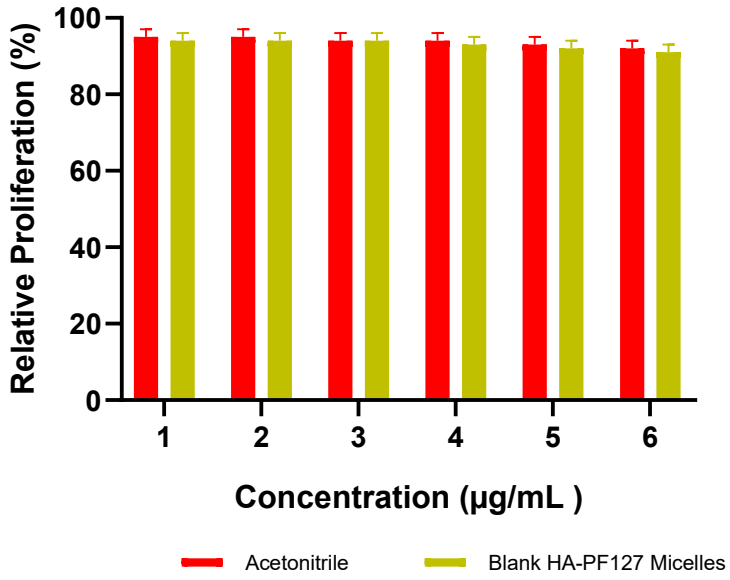

(A)

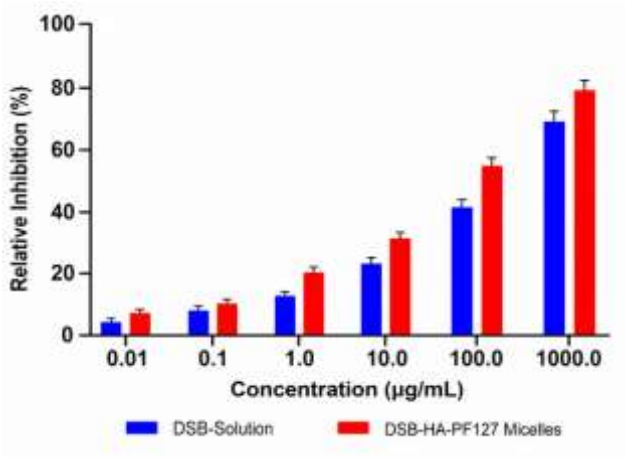

(B)

Figure 9: *In vitro* cytotoxicity of acetonitrile and blank-HA-PF127 micelles on human breast adenocarcinoma cells (MCF-7) after 72 h. A) Effect on relative proliferation of MCF-7 cell line after treatment with different concentration of samples. The bars represent mean±SD (n = 3). *In vitro* cytotoxicity of DSB-HA-PF127 micelles and DSB solution (free drug) on human breast adenocarcinoma cells (MCF-7) after 72 h, B) showing effect of different concentration of DSB solution and DSB-HA-PF127 micelles. The bars represent mean±SD (n = 3)

Stability study

The development of formulation requires a stability study, which is useful in demonstrating the product's quality under the influence of changing environmental conditions over time. According to ICH recommendations, the stability investigation of the optimised DSB-HA-PF127 micelle formulation was conducted for three months at room temperature, freezing temperature, and 40 ± 2 °C with 75 ± 5% relative humidity (RH) as quoted in **Table 6, 7** and 8**,** respectively.

Table 6: Stability study data for DSB-HA-PF127 micelles at 40 ± 2 °C, 75 ± 5% RH

Sr. No.	Stability study parameters	Initial	After 3 months
1	Phase separation	No Phase separation	No Phase separation
2	Drug content (%)	94.70 ± 1.2	95.34 ± 0.67
3	Particle size (nm)	149.9±2.58	154.3±1.0

Table 7: Stability study data for DSB-HA-PF127 micelles at room temperature

Sr. No.	Stability study parameters	Initial	After 3 months
1	Phase separation	No Phase separation	No Phase separation
2	Drug content (%)	94.70 ± 1.2	96.86 ± 0.83
3	Particle size (nm)	149.9±2.58	152.2±1.25

Table 8: Stability study data for DSB-HA-PF127 micelles at freezing temperature

Sr. No.	Stability study parameters	Initial	After 3 months
1	Phase separation	No Phase separation	No Phase separation
2	Drug content (%)	94.70 ± 1.2	96.0 ± 0.57
3	Particle size (nm)	149.9±2.58	150.5± 1.0

CONCLUSION

Based on the overall findings from the cytotoxicity study in human breast adenocarcinoma cells (MCF-7), zeta potential, scanning electron microscopy, entrapment efficiency, and in vitro drug release study, it was determined that the DSB-HA-PF127 micelles have a greater potential for use as a administering medication vehicle owing to their distinctive capacity to incorporate hydrophobic drugs into their own personal space, their less sized particles at the at the nanoscale, and their medication delivery under strict oversight. Strong experimental support is provided by this study for the creation of DSB-HA-PF127 micelles as a successful strategy for creating a regulated drug delivery system for anticancer medications with enhanced stability.

REFERENCE

1. Lindauer, M., Hochhaus, A. (2014). Dosatinib. In: Martens, U. (eds) Small Molecules in Oncology. Recent Results in Cancer Research, vol 201. Springer, Berlin, Heidelberg. https://doi.org/10.1007/978-3-642-54490-3_2
2. Smita Tukaram Kumbhar, Ravikant Yashwantrao Patil, Manish Sudesh Bhatia, Prafulla Balkrushna Choudhari, Vinod Limbraj Gaikwad, Synthesis and characterization of chitosan nanoparticles decorated with folate and loaded with Dosatinib for targeting folate receptors in cancer cells,Open Nano, Volume7,2022,100043, ISSN2352-9520, https://doi.org/10.1016/j.onano.2022.100043.
3. Urvi H. Gala, Dave A. Miller, Robert O. Williams,Harnessing the therapeutic potential of anticancer drugs through amorphous solid dispersions,Biochimica et Biophysica Acta (BBA) - Reviews on Cancer,Volume 1873, Issue 1,2020,188319,ISSN 0304-419X, https://doi.org/10.1016/j.bbcan.2019.188319.
4. Ahmed A. Abdelgalil, Mohd. Aftab Alam, Mohammad Raish, Imad Eldin Mohammed, Abd-Elwahab Hassan Mohammed, Mushtaq Ahmad Ansari, Fahad I. Al Jenoobi,Dosatinib significantly reduced in vivo exposure to cyclosporine in a rat model: The possible involvement of CYP3A induction,Pharmacological Reports,Volume 71, Issue 2, 2019, Pages 201-205, ISSN 1734-1140, https://doi.org/10.1016/j.pharep.2018.10.018.
5. Sally A. Sabra, Salah A. Sheweita, Medhat Haroun, Doaa Ragab, Maha A. Eldemellawy, Ying Xia, David Goodale, Alison L. Allan, Ahmed O. Elzoghby, Sohrab Rohani, Magnetically Guided Self-Assembled Protein Micelles for Enhanced Delivery of Dosatinib to Human Triple-Negative Breast Cancer Cells, Journal of Pharmaceutical Sciences, Volume 108, Issue 5,2019, Pages 1713-1725, ISSN 0022-3549, https://doi.org/10.1016/j.xphs.2018.11.044.
6. Yiyao Liu, Hirokazu Miyoshi, Michihiro Nakamura, Encapsulated ultrasound microbubbles: Therapeutic application in drug/gene delivery, Journal of Controlled Release, Volume 114, Issue 1,2006, Pages 89-99, ISSN 0168-3659, https://doi.org/10.1016/j.jconrel.2006.05.018.
7. Ye Wang, Xiang Li, Yan Zhou, Pengyu Huang, Yuhong Xu, Preparation of nanobubbles for ultrasound imaging and intracelluar drug delivery, International Journal of Pharmaceutics, Volume 384, Issues 1–2,2010, Pages 148-153, ISSN 0378-5173, https://doi.org/10.1016/j.ijpharm.2009.09.027.

8. Lisa Brannon-Peppas, James O. Blanchette, Nanoparticle and targeted systems for cancer therapy, Advanced Drug Delivery Reviews, Volume 56, Issue 11,2004, Pages 1649-1659, ISSN 0169-409X, https://doi.org/10.1016/j.addr.2004.02.014.
9. Xuemei Zhang, Yuanyi Zheng, Zhigang Wang, Shuai Huang, Yu Chen, Wei Jiang, Hua Zhang, Mingxia Ding, Qingshu Li, Xiaoqiu Xiao, Xin Luo, Zhibiao Wang, Hongbo Qi,Methotrexate-loaded PLGA nanobubbles for ultrasound imaging and Synergistic Targeted therapy of residual tumor during HIFU ablation,Biomaterials,Volume 35, Issue 19,2014,Pages 5148-5161,ISSN 0142-9612, https://doi.org/10.1016/j.biomaterials.2014.02.036.
10. Jeff S. Xu, Jiwei Huang, Ruogu Qin, George H. Hinkle, Stephen P. Povoski, Edward W. Martin, Ronald X. Xu,Synthesizing and binding dual-mode poly (lactic-co-glycolic acid) (PLGA) nanobubbles for cancer targeting and imaging,Biomaterials,Volume 31, Issue 7,2010, Pages 1716-1722, ISSN 0142-9612, https://doi.org/10.1016/j.biomaterials.2009.11.052.
11. Betty Tyler, David Gullotti, Antonella Mangraviti, Tadanobu Utsuki, Henry Brem,Polylactic acid (PLA) controlled delivery carriers for biomedical applications,Advanced Drug Delivery Reviews,Volume 107,2016,Pages 163-175,ISSN 0169-409X,https://doi.org/10.1016/j.addr.2016.06.018.
12. Mohammad Ashad Ghani Nasim, Osama Khan, Mohd Parvez, Bhupendra Kumar Bhatt,Optimizing ultrasonic reactor operating variables using intelligent soft computing models for increased biodiesel production,Green Technologies and Sustainability,Volume 1, Issue 3,2023,100033,ISSN 2949-7361, https://doi.org/10.1016/j.grets.2023.100033.
13. Lindauer M, Hochhaus A. Dosatinib. Recent Results Cancer Res. 2014;201:27-65. doi: 10.1007/978-3-642-54490-3_2. PMID: 24756784.
14. Roy S, Quiñones R, Matzger AJ. Structural and Physicochemical Aspects of Dosatinib Hydrate and Anhydrate phases. Cryst Growth Des. 2012 Apr 4;12(4):2122-2126. doi: 10.1021/cg300152p. Epub 2012 Mar 13. PMID: 23472049; PMCID: PMC3586737.
15. Ségaliny AI, Tellez-Gabriel M, Heymann MF, Heymann D. Receptor tyrosine kinases: Characterisation, mechanism of action and therapeutic interests for bone cancers. J Bone Oncol. 2015 Jan 23;4(1):1-12. doi: 10.1016/j.jbo.2015.01.001. PMID: 26579483; PMCID: PMC4620971.
16. Kishore Kumar Boddu, Kumar Shiva Gubbiyappa, Multi-factor optimization and interaction analysis for enhanced nanobubble formulation and performance of Dosatinib, Journal of Drug Delivery Science and Technology, Volume 101, Part A, 2024, 106112, ISSN 1773-2247, https://doi.org/10.1016/j.jddst.2024.106112.